LA-UR 97-2212

Los Alamos National Laboratory is operated by the University of California for the United States Department of Energy under contract W-7405-ENG-36.

CONF-970657--3

TITLE: GROWTH RATE AND TRANSITION TO TURBULENCE OF A GAS CURTAIN

AUTHOR(S): Peter V. Vorobieff

Paul M. Rightley

Robert F. Benjamin

SUBMITTED TO International Workshop on the Physics of Compressible Turbulent Mixing (Marseille, France, 18-21 June 1997)

DISCLAIMER

Portions of this document may be illegible in electronic image products. Images are produced from the best available original document.

Growth Rate and Transition to Turbulence of a Gas Curtain

P. Vorobieff*, P. Rightley and R. Benjamin
Los Alamos National Laboratory, group DX-3
Los Alamos, NM 87545, USA

Abstract: We conduct shock-tube experiments to investigate Richtmyer-Meshkov (RM) instability of a narrow curtain of heavy gas (SF_6) embedded in lighter gas (air). Initial perturbations of the curtain can be varied, producing different flow patterns in the subsequent evolution of the curtain. Multiple-exposure video flow visualization provides images of the growth of the instability and its transition to turbulence, making it possible to extract quantitative information such as the width of the perturbed curtain. We demonstrate that the width of the curtain with initial perturbation on the downstream side is non-monotonic. As the initial perturbation undergoes phase inversion, the width of the curtain actually decreases before beginning to grow as the RM instability evolves.

1. Introduction

Ricthmyer-Meshkov instability [1, 2] is the impulsively-driven analog of the well-known Rayleigh-Taylor instability. Understanding and quantification of the evolution of RM instability is important in many fields ranging from astrophysics [3, 4] to high-speed combustion [5] and inertial confinement fusion [6]. There also has been a significant interest to numerical simulations of RM instability [7]. The present study provides both the qualitative information on the flow morphology during the instability growth and the measurements of the thickness of the mixing layer associated with the instability. The latter also serve as benchmarks for CFD codes.

Earlier experimental studies [8, 9, 10] revealed the existence of three basic flow patterns in the evolution of a shock-accelerated heavy gas curtain embedded in a lighter gas. Both the upstream and the downstream interfaces of the curtain are Richtmyer-Meshkov unstable. At the upstream interface the shock front moves across a positive density gradient, and the initial sinusoidal perturbation of the interface begins to grow immediately after shock compression, producing the flow pattern known as the upstream mushrooms. If similar perturbations are initially present at the downstream interface, where the shock front traverses a negative density gradient, the perturbations must first reverse phase and then grow, evolving into the pattern known as the downstream mushrooms. If both sides of the curtain are perturbed and its initial cross-section is varicose, the downstream interface perturbation likewise reverses phase, leading to formation of the sinuous flow pattern. Earlier studies did not possess the temporal resolution to detect the narrowing of the gas curtain corresponding to phase reversal of the downstream interface. Initially only one or two successive exposures per one-millisecond event of shock–gas curtain interaction were captured, and our more recent investigation [11] provided 8–10 images per event. The present study increases the temporal resolution to 30–32 images per event. With this resolution, it becomes possible to observe non-monotonic growth of the mixing layer for the case of the gas curtain with the initially perturbed downstream side.

*Email: kalmoth@lanl.gov, WWW: http://cnls-www.lanl.gov/~azathoth/dx3.html

2. Experimental setup and techniques

Our experiments employed a 5.5 m horizontal shock tube with internal dimensions of 75 mm square producing a Mach 1.2 planar shock wave. The driver section and the driven section (which is kept at ambient pressure) are separated by a membrane of three thin sheets of polypropylene which are punctured by a solenoid-actuated spike. Two flush-mounted pressure transducers mounted near the downstream end of the driven section monitored shock quality and speed. One final transducer just upstream of the test section triggers the diagnostics.

A curtain of heavy gas (sulfur hexafluoride, nominal density at ambient pressure about 5 times that of air) flows vertically through the test section. The curtain enters the test section through a contoured nozzle. Microscopic water/glycol droplets are produced with a modified theatrical fog generator and mixed with the heavy gas. The mean size of the droplets is estimated to be 0.5 μm; the cloud of droplets does not contribute any significant mass loading. After flowing vertically downward through the test section, the gas curtain is removed from the shock tube by a vacuum system. The contoured nozzle through which the gas curtain enters the shock tube provides the desired initial conditions. The vertical motion of the gas curtain does not provide a significant perturbation to the motion of the flow on the timescales of interest. Also, the slow temporal evolution of the gas curtain provides a rich variety of initial conditions, but also eliminates shot-to-shot reproducibility. This requires that a s ignificant amount of data be obtained for each event if the time evolution of the flow is to be characterized. The experimental apparatus and diagnostics are discussed in greater detail elsewhere [11].

Laser-knife flow visualization employed a 1 W Ar+ (Lexel Model 94) laser. To achieve maximum temporal resolution, we recorded the evolution of the flow in the plane of the laser knife (parallel to the direction of shock propagation and perpendicular to the gas curtain) with a Hadland Photonics 468 video camera. This camera is composed of eight individual MCP intensified CCD cameras arranged to use a single optical axis. The gas curtain is thin and travels downstream after shock acceleration, making it possible to acquire up to four exposures on each CCD with a pulsed optical intensifier. Thus the total number of successive exposures of the curtain thart can be acquired in one experiment is 32. Each of the CCD cameras internal to the 468 is independently programmable, and the camera as a whole is triggered by the third pressure transducer just upstream of the test section.

3. Observations

Figure 1 shows the typical evolutionary sequence of the downstream mushroom flow pattern. The leftmost exposure (1 in the figure) shows the initial condition with the prevailing perturbation on the downstream side and with one wavelength (6 mm) defining the perturbation. The following exposures are acquired starting with the beginning of the interaction of the shock wave with the curtain. Time intervals between exposures 2 to 14 are 20 μs, and 40 μs for later exposures. The duration of each exposure is 10 μs.

The initial compression and phase inversion of the downstream interface lead to noticeable thinning of the curtain in exposures 2–4 and flattening of the downstream boundary. Subsequent exposures show the growth of the perturbation and formation of mushroom-like shapes formed by the curtain material rolling up around the vortices deposited by the interaction of the shock with the curtain [11](exposures 12–15). Until exposure 15, there is little or no evidence of interaction between the individual wavelengths of the curtain; however, later mode-coupling becomes evident, as well as emergence of small-scale spatial structures.

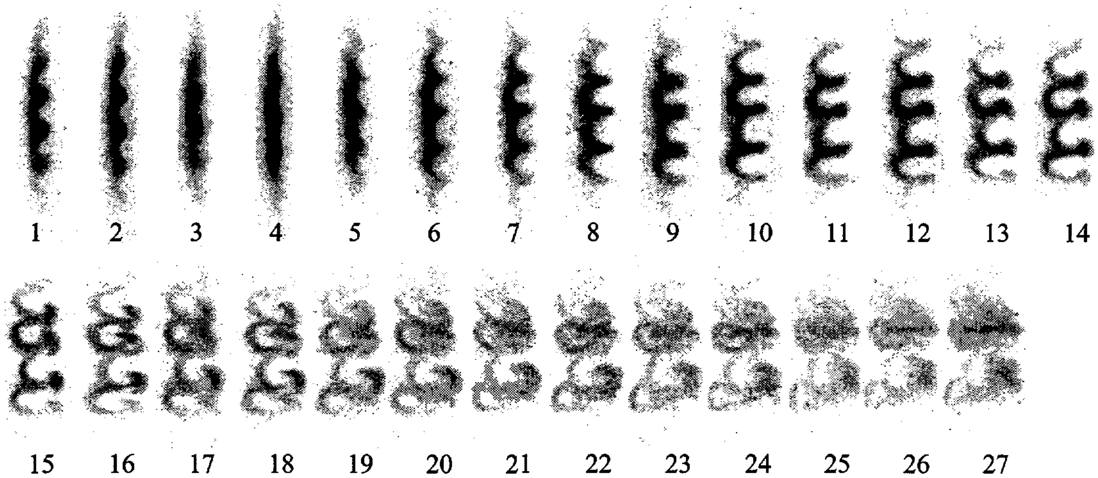

Figure 1. Evolution of downstream mushroom flow pattern. One wavelength (6mm) was present in initial perturbation.

Figure 2 shows the evolution of upstream mushrooms from initial conditions with upstream-side perturbation prevailing. In this image sequence, there were two wavelengths initially present. Time interval between exposures 1–13 is 20 μs, and 40 μs for subsequent exposures. Unlike the downstream mushrooms in Figure 1, upstream mushrooms begin growing immediately after the shock compresses the curtain (exposure 2), and smaller spatial structures indicative of transition to turbulence are more prominent than in the previous data set.

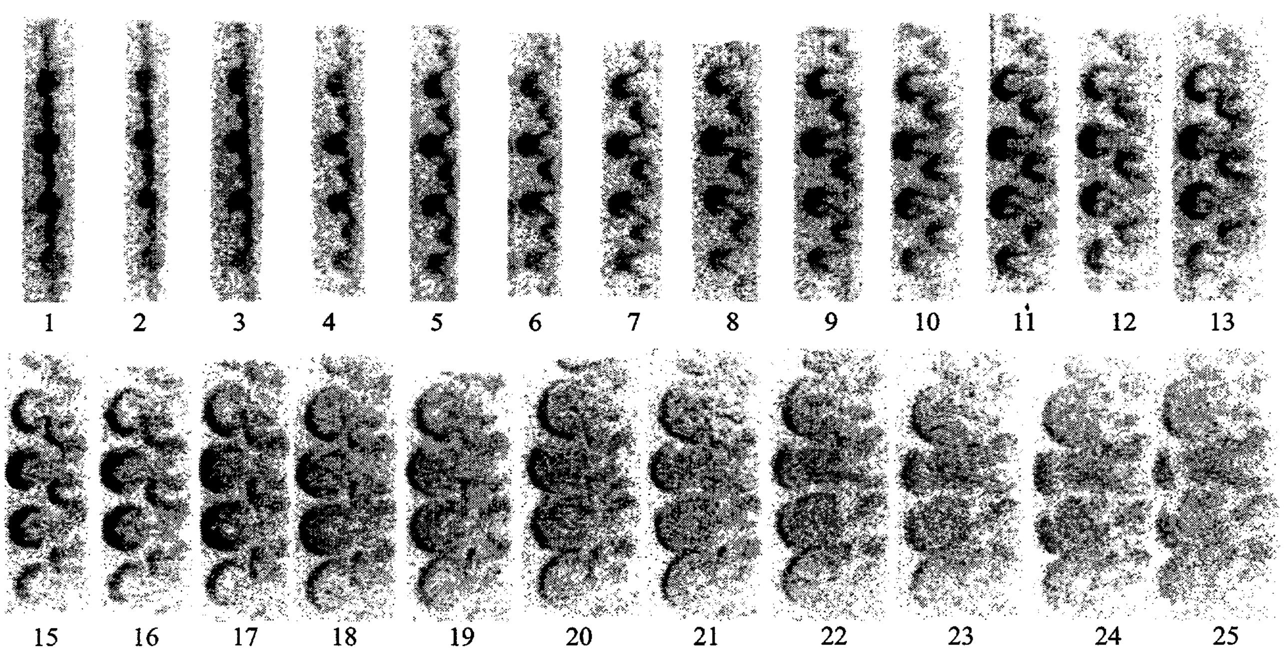

Figure 2. Evolution of upstream mushroom flow pattern with two wavelengths present in initial perturbation.

4. Analysis

The image sequence in Figure 1 shows that at the early stages of the evolution of the downstream mushroom flow pattern the width of the gas curtain decreases. In Figure 3, time history of the widths of the individual wavelengths of the curtain is plotted for this image sequence. The picture in the bottom right corner of the graph shows the image of the initial conditions and the schematic depicting how the width per wavelength is measured. The measurement procedure is described in detail elsewhere [11]. Widths of all three wavelengths measured have a local minimum at the time approximately 40 μs after the shock hits the curtain.

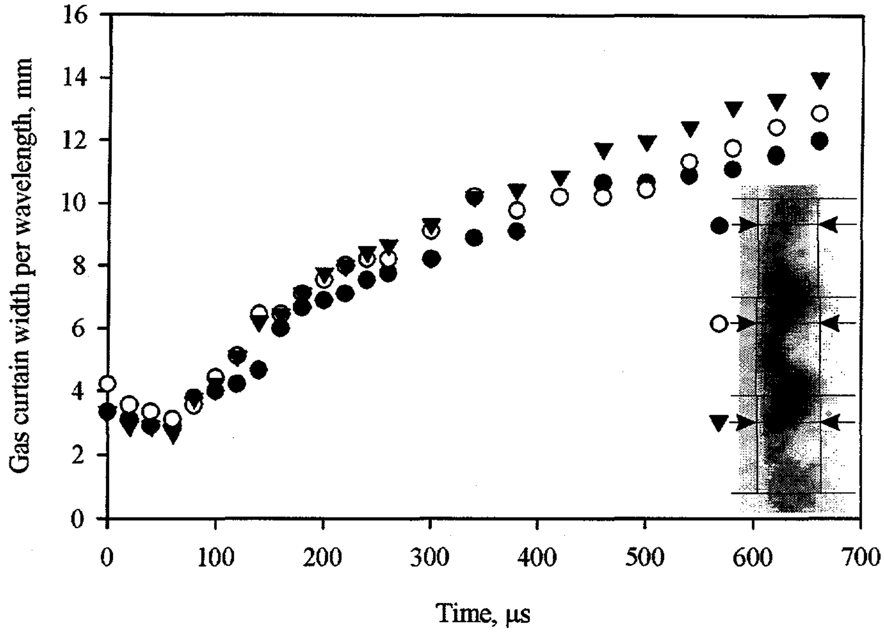

Figure 3. Width of the perturbed gas curtain per wavelength vs. time, downstream mushrooms. Schematic shows measurement of curtain width for individual wavelengths.

A simple model that approximates vorticity deposited by the shock interaction with the curtain as an infinite row of point vortices and assumes initial symmetry of the layer and vorticity distribution [10] is clearly not adequate for the description of the evolution of downstream mushrooms, because this model predicts monotonic growth. However, qualitatively the graphs closely resemble those produced with a simplified vortex-blob numerical simulation that neglects density gradients or compressibility but uses finite Gaussian vortex cores and takes into account the asymmetric initial conditions and resulting asymmetry in the deposition of vorticity [11].

Another interesting feature of the graph is that at times earlier than 400 μs perturbation in the first wavelength (•) grows faster than that in the second wavelength (○), while at later times the amplitude of the second wavelength exceeds that of the first wavelength. This may be the effect of wavelength interaction and mode coupling.

5. Conclusion

With the recent refinements of the gas-curtain experimental technique, now it is possible to acquire more than thirty images of the evolution of the gas curtain during and after the shock interaction. The temporal resolution of 20 μs between subsequent exposures is sufficient to resolve the phase inversion on the downstream interface of the curtain resulting, in the case of the downstream mushroom flow morphology, in delay in the growth of the perturbations in the curtain. There is also more evidence of both mode-coupling and emergence of smaller spatial scales at later stages of evolution, eventually leading to turbulence.

Acknowledgement. This work is supported by DOE contract No. W–7405–ENG–36. One of the authors is partially supported by the Center for Nonlinear Studies (CNLS) at Los Alamos National Laboratory.

References

[1] Richtmyer RD, Taylor instability in shock acceleration of compressible fluids, *Commun. Pure Appl. Maths.* **23**, 297-319 (1960).

[2] E.E. Meshkov, Instability of a shock wave accelerated interface between two gases, NASA TT F-13, 074 (1970).

[3] Burrows A, Hayes J and Fryxell BA, On the nature of core-collapse supernova explosions, *Astrophys. J.* **450**, 830 (1995).

[4] Stone JM, Xu J and Mundy LG, Formation of 'bullets' by hydrodynamical instabilities in stellar outflows, *Nature (London)* **377**, 315-317 (1995).

[5] Markstein GH, A shock tube study of flame front-pressure wave interaction, *6th International Symposium on Combustion*, Reinhold, 387-398 (1957).

[6] Sunahara A, Takeuchi H, Takabe H, and Mima K, Effects of multiple shock and thermal conduction on mixing layer evolution in a stagnating high-gain inertial confinement fusion TA, *Jap. Journ. App. Phys.* Part 1, **35**, 6265-6272 (1996).

[7] Baltrusaitis RM, Gittings ML, Weaver RP, Benjamin RF and Budzinski JM, Simulation of shock-generated instabilities, *Phys. Fluids* **8**, 2471-2483 (1996).

[8] Jacobs JW, Klein DL, Jenkins DG and Benjamin RF, Instability growth patterns of a shock-accelerated thin fluid layer, *Phys. Rev. Lett.* **70**, 583-586 (1993).

[9] Budzinski JM, Benjamin RF and Jacobs JW, Influence of initial conditions on the flow patterns of a shock-accelerated thin fluid layer, *Phys. Fluids* **6**, 3510-3512 (1994).

[10] Jacobs JW, Jenkins DG, Klein DL and Benjamin RF, Nonlinear growth of the shock-accelerated instability of a thin fluid layer, *J. Fluid Mech.* **295**, 23-42 (1995).

[11] Rightley PM, Vorobieff P, and Benjamin RF, Evolution of a shock-accelerated thin fluid layer, *Phys. Fluids* **9**, 1770-1782 (1997).